is no evidence for a region of structures due to autoionization below the obvious onset in the spectrum for the production of $(C_4H_8 \cdot SO_2)^+$ in Figure 5, so we assume that our reported value for $D_0([C_4H_8 \cdot SO_2]^+)$ corresponds to the ground state of the ionic complex.

There are a number of limitations to the technique described herein that must be acknowledged. (1) Normalization of the two spectra in preparation for subtraction requires that the threshold for photoionization of A be characterized by a distinctive feature. (2) The approximately linear threshold for dissociative photoionization of the dimer requires a step-function onset for photoionization of A. When the photoionization of A displays only a weak and indistinct onset, the present technique is inadequate. (3) Autoionization features in the threshold function for dissociative photoionization of the dimer could distort its linearity. (4) If $D(A \cdot B)$ is too small, the interval between the ionization potential of A and the appearance potential of A^+ from A·B becomes too narrow to allow the necessary normalization of the spectra to be carried out. This establishes a practical lower limit of roughly 1 kcal mol^{-1} (0.04 eV) for dissociation energies that can be measured with our apparatus. It should be noted that dimers of this or lower dissociation energies can readily be made in useful densities by suitable adjustment of nozzle design and expansion conditions. (5) Optimization of the dimer density and minimization of the interference from trimers determines the beam temperature, so there is always a correction for the beam temperature in passing from the measured dissociation energy to the dissociation energy at 0 K, the uncertainty of which correction increases the uncertainty that must be cited for the measurement. (6) As already discussed, if the target beam contains more than one isomer of the dimer in important amounts, the measured dissociation energy will likely be that of the least bound one. (7) The process $A \cdot B + h\nu \rightarrow A^+ + B + e$ must proceed with sufficiently large cross sections in the threshold region to allow its efficiency function to be resolved from the statistical scatter of measured points after the normalization and subtraction have been carried out. Our attempt to measure the dissociation energy of the benzene dimer was not successful because the cross sections are too small. As already explained above, small cross sections are to be expected whenever the dissociation energy of the dimer ion $(A \cdot B)^+$ is large, e.g., whenever $D([A \cdot B]^+) > 15$ kcal mol^{-1}. However, small cross sections can also occur for some other reason(s) that is(are) not yet understood. (8) Other potential problems that can be foreseen are effects due to ion pair formation, hot bands, delayed ion dissociation, and nonexistence of a stable A^+ (e.g. if $A = SF_6$).

Acknowledgment. We wish to thank the NSLS/HFBR Faculty-Student Support Program for travel funds to make this work possible. This research was carried out at Brookhaven National Laboratory under Contract DE-AC02-76CH00016 with the U.S. Department of Energy and supported by its Division of Chemical Sciences, Office of Basic Energy Sciences. We also thank E. T. Hui and P. F. Fernandez for assistance with the experiments. This work was performed while one of us (E.A.W.) was on sabbatical leave from the University of New Mexico.

Photodissociation of the Dimanganese Ion, Mn_2^+: A Route to the Energetics of Metal Clusters

Martin F. Jarrold, Andreas J. Illies,† and Michael T. Bowers*

Contribution from the Department of Chemistry, University of California, Santa Barbara, California 93106. *Received May 16, 1985*

Abstract: The results of a study of the photodissociation of the dimanganese ion (Mn_2^+) in the visible region of the spectrum (477–590 nm) are reported. Experiments were performed using a crossed high-energy ion beam/laser beam apparatus. Photofragment relative kinetic energy distributions and angular distributions are reported. The kinetic energy distributions show two components which were assigned to ground and excited electronic state products. The angular distributions are characterized by an asymmetry parameter of $\beta = 0.4 \pm 0.1$ which indicates photodissociation does not occur via a direct transition to a repulsive excited state. The interpretation of kinetic energy thresholds in the photofragment distributions leads to a rigorous lower limit for the metal–metal bond energy of Mn_2^+ of $D^\circ_0(Mn^+\text{–}Mn) \geq 1.39$ eV (32 kcal mol^{-1}) and an upper limit for the ionization potential of the neutral dimer of $IP(Mn_2) \leq 6.47$ eV.

I. Introduction

Metal clusters have been the subject of a rapidly expanding research effort over the past 2 or 3 years.[1-11] Studies of metal clusters impact on a diverse range of both applied and fundamental research areas. These include catalysis and its relationship with studies of well-characterized surfaces as well as microelectronics and solid-state physics, particularly with regard to understanding the emergence of bulk properties such as metallic conductivity and band structure.

Metal clusters have been studied in matrices and in the gas phase. Recent interest has focused more on gas-phase studies, in part because of the inherent difficulty of the matrix studies.[1] However, studying metal clusters in the gas phase is not easy owing to the difficulty in generating the clusters. With the exception of the alkali metals, most metals are refactory. Hence, high-temperature ovens[2] or pulsed laser evaporation[3] are required to

†Present address: Department of Chemistry, Auburn University, Auburn, AL 36849.

(1) See, for example: Ozin, G. A., *Faraday Symp. Chem. Soc.* **1980**, *14* 7. DiLella, D. P.; Limm, W.; Lipson, R. H.; Moskovits, M.; Taylor, K. V. *J. Chem. Phys.* **1982**, *77*, 5263. Baumann, C. A.; Van Zee, R. J.; Weltner, W. *Ibid.* **1983**, *79*, 5272. Bondybey, V. E.; English, J.H. **1980**, *72*, 6479.

(2) Riley, S. J.; Parks, E. K.; Mao, C.-R.; Pobo, L. G.; Wexler, S. *J. Phys. Chem.* **1982**, *86*, 3911.

(3) Dietz, T. G.; Duncan, M. A.; Powers, D. E.; Smalley, R. E. *J. Chem. Phys.* **1981**, *74*, 6511. Bondybey, V. E. *J. Phys. Chem.* **1982**, *86*, 3396.

(4) See, for example: Hopkins, J. B.; Langridge-Smith, P. P. R.; Morse, M. D.; Smalley, R. E. *J. Chem. Phys.* **1983**, *78*, 1627. Bondybey, V. E.; Heaven, M.; Miller, T. A. *Ibid.* **1983**, *78*, 3593. Bondybey, V. E.; English, J. H. *Ibid.* **1983**, *79*, 4746. Morse, M. D.; Hopkins, J. B.; Langridge-Smith, P.R.R.; Smalley, R. E. *Ibid.* **1983**, *79*, 5316.

(5) See, For example: Riley, S. J.; Parks, E. K.; Nieman, G. C.; Pobo, L. G.; Wexler, S., *J. Chem. Phys.* **1984**, *80*, 1360. Geusic, M. E.; Morse, M. D.; Smalley, R. E. *Ibid.* **1985**, *82*, 590. Whetten, R. L.; Cox, D. M.; Trevor, D. J.; Kaldor, A. *Ibid.* **1985**, *89*, 566.

0002-7863/85/1507-7339$01.50/0

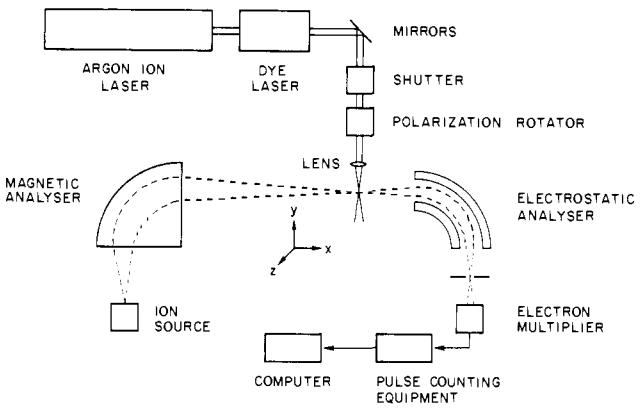

Figure 1. Schematic diagram of the experimental apparatus. Note that the laser beam is actually along the z axis (vertical) as it intersects the ion beams.

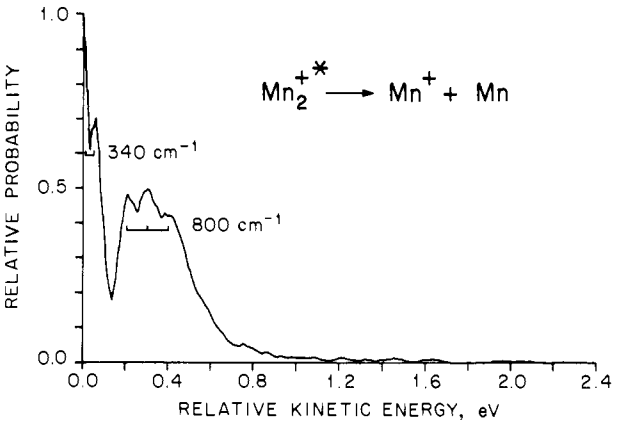

Figure 2. Product relative kinetic energy distribution for the unimolecular "metastable" dissociation of Mn_2^{+*}.

generate the clusters. Studies of the metal clusters are further complicated by the fact that a range of different cluster sizes are generated, making it difficult to study the properties as a function of size. To date, the spectroscopy of a number of small clusters, almost exclusively dimers, have been studied in the gas phase[4] and the qualitative reactivity of bare metal clusters with some simple molecules investigated.[5]

In this paper we report the results of a study of the photodissociation of the dimanganese ion (Mn_2^+). Studying cluster ions rather than their neutral counterparts offers several advantages. First, it is possible to mass select a specific species for detailed study so that studies can readily be performed as a function of cluster size. Second, detection does not involve ionization with the ensuing complications of unknown ionization cross sections and possible fragmentation. To date, studies of metal cluster ions have been mainly concerned with investigating the chemistry of small bare metal clusters, usually dimers, and metal clusters with ligands, usually CO.[6]

The Mn_2^+ ion is particularly interesting because it has an electronic configuration intermediate between Cr_2 and Mn_2, both of which have been studied spectroscopically. Cr_2, which is bound by 1.56 ± 0.20 eV,[7] has an extremely short bond length (1.68 Å) and perhaps a sextuple metal–metal bond.[8] Its next-door neighbor in the periodic table, Mn_2, is bound by only 0.43 ± 0.30 eV,[7] has a long bond length (~3.4 Å), and has been described as a van der Waals molecule.[9] Information about the Mn_2^+ ion may be useful in helping to unravel the details of the bonding in the series Cr_2, CrMn, Mn_2^+, Mn_2.

The Mn_2^+ ions studied here were generated by electron impact on $Mn_2(CO)_{10}$. Generating metal clusters by electron impact on organometallics is easier than oven techniques or pulsed laser evaporation, but not as general. $Mn_2(CO)_{10}$ is a relatively easy compound to handle so the Mn_2^+ ion has been studied on several occasions. Armentrout and co-workers have used collision-induced dissociation to obtain a value for the dissociation energy of Mn_2^+.[10] Both Armentrout and co-workers and Ridge and co-workers have investigated the reactivity of Mn_2^+.[11]

II. Experimental Section

The experiments were performed using a crossed ion beam–laser beam apparatus which is described in detail elsewhere.[12-14] The experimental apparatus, shown schematically in Figure 1, consists of a reverse geometry mass spectrometer (VG Analytical, ZAB-2F), an argon ion laser (Coherent, Innova 20), and broad-band dye laser (Coherent, Model 590). Briefly, the overall operation of this experimental apparatus is as follows. Ions, generated in the ion source, are accelerated to 8 kV and mass selected by the magnet. The mass selected ion beam is then crossed with the focused laser beam and the products are analyzed by an electrostatic analyzer (ESA).

$Mn_2(CO)_{10}$ is a solid with a relatively low vapor pressure at room temperature. In order to generate a sufficient pressure of $Mn_2(CO)_{10}$ in the source for long periods of time, we developed a temperature-variable EI/CI (electron impact/chemical ionization) ion source with a solids inlet probe. $Mn_2(CO)_{10}$ (Alfa Products) was loosely packed into the solids inlet probe which is essentially a tube, closed at one end, with internal dimensions: 2.0 mm diameter and 16.5 mm long. Before inserting the probe into the source, the source was precooled by flowing cold nitrogen through the CuBe source block. The probe was then inserted into the source through a differentially pumped inlet valve, and the source temperature slowly raised to around 50 °C. This temperature gave an adequate pressure of $Mn_2(CO)_{10}$ in the source (around 10^{-4} torr).

Mn_2^+ ions were generated by 100-eV electron impact. The Mn_2^+ ion was found to be the most intense peak in the low-pressure EI mass spectrum of $Mn_2(CO)_{10}$ under the conditions employed. (The relative intensities in the mass spectrum of $Mn_2(CO)_{10}$ apparently vary substantially with the conditions employed.[15]) The resulting Mn_2^+ ion beam was estimated to be around 10^{-10} Å and was stable for around 9 h until the probe needed refilling with $Mn_2(CO)_{10}$. For most of the experiments the ion source was operated in the EI mode (with a 1.5 mm × 5 mm exit slit and pressures around 10^{-4} torr). Some measurements were performed with an N_2 (liquid boil-off) buffer gas with the source operated in the CI mode (with a 0.1 mm × 5.5 mm exit slit and pressures around 0.06 torr).

Product peaks were recorded using pulse counting techniques in a multichannel analyzer (1 eV per channel) which was scanned in synchronization with the ESA voltage. An energy resolving power of 2000 (fwhm) was employed. A fairly large background signal (around 10^3 counts s^{-1}) was present with the laser beam off. This signal arose from the "metastable" dissociation of a small fraction of the Mn_2^+ ions in the beam which were in a long-lived excited electronic state. We will discuss this "metastable" dissociation in more detail below. For the photodissociation studies the background signal was removed by modulating the laser beam and utilizing up–down counting.

The data reported here were recorded with the discrete lines of the argon ion laser and with the dye laser using R6G dye. An important feature of the crossed laser/fast ion beam experiment is that it is possible to change the orientation of the laser beam polarization with respect to the ion beam direction and obtain information on the product angular distributions. Both laser beams are plane polarized and the orientation of the laser beam polarization was changed using a polarization rotator (Spectra Physics, 310A). Measurements were performed with the polarization at 0, 90°, and at the "magic angle" of 54.7° with respect to the ion beam direction, for reasons which will become clear below.

(6) See, for example, Freas, R. B.; Ridge, D. P. *J. Am Chem. Soc.* **1980**, *102*, 7129. Jacobson, D. B.; Freiser, B. S. *Ibid.* **1984**, *106*, 4623. Anderson Fredeen, D.; Russell, D. H. *Ibid.*, in press.
(7) Gingerich, K. A. *Faraday Symp. Chem. Soc.* **1980**, *14*, 109.
(8) Michalopoulos, D. L.; Geusic, M. E.; Hansen, S. G.; Powers, D. E.; Smalley, R. E. *J. Phys. Chem.* **1982**, *86*, 3914.
(9) Bauman, C. A.: Van Zee, R. J.; Bhat, S. V.; Weltner, W. *J. Chem. Phys.* **1983**, *78*, 190.
(10) Ervin, K.; Loh, S. K.; Aristov, N.; Armentrout, P. B. *J. Phys. Chem.* **1983**, *87*, 3593.
(11) Armentrout, P. B.; Loh, S. K.; Ervin, K. M. *J. Am. Chem. Soc.* **1984**, *106*, 1161. Larsen, B. S.; Freas, R. B.; Ridge, D. P. *J. Phys. Chem.* **1984**, *88*, 6014.
(12) Jarrold, M. F.; Illies, A. J.; Bowers, M. T. *J. Chem. Phys.* **1983**, *79*, 6086.
(13) Jarrold, M. F.; Illies, A. J.; Bowers, M. T. *J. Chem. Phys.* **1984**, *81*, 214.
(14) Jarrold, M. F.; Illies, A. J.; Bowers, M. T. *J. Chem. Phys.* **1985**, *82*, 1832.
(15) Litzow, M. R.; Spalding, T. R. "Mass Spectrometry of Inorganic and Organometallic Compounds"; Elsevier: Amsterdam, 1973.

III. Results

A. Unimolecular Metastable Dissociation of Mn_2^+. As noted in the Experimental Section a fairly strong background signal was present with the laser off. This signal arose from a fraction of the Mn_2^+ ions in the beam that underwent spontaneous unimolecular dissociation between the magnet and ESA. Collision-induced dissociation of the Mn_2^+ parent ion resulted in a significantly different peak shape for the Mn^+ product, which indicates that the background signal arose from a true unimolecular process. The product relative kinetic energy distribution derived from the metastable peak shape[16] is shown in Figure 2. The distribution shows several reproducible features: two sharp peaks separated by around 340 cm^{-1} at close to zero relative kinetic energy and three broader peaks separated by close to 800 cm^{-1} at around 0.3 eV relative kinetic energy.

B. Photofragment Angular Distributions. The products of photodissociation are generally not distributed isotropically. They have an angular disribution given by [17]

$$P(\theta) = (4\pi)^{-1}[1 + \beta P_2(\cos\theta)] \quad (1)$$

in which $P(\theta)$ is the probability that products recoil into a solid angle $d\omega$ at an angle θ with respect to the electric vector; $P_2(\cos\theta)$ is the second degree Legendre polynomial; and β is the asymmetry parameter. Photofragment angular distributions provide information on the polarization of the electronic transition and on the lifetime of the excited ion relative to a rotational period.[17] In our experiment information on the product angular distribution is obtained from measurements with the laser beam polarization at 0 and 90° with respect to the ion beam direction. The ESA measures essentially the energy component along the ion beam direction. If the products recoil preferentially along the electric vector, a broad peak will be measured with the laser polarization along the ion beam direction and a narrow peak measured with the laser polarization perpendicular to the ion beam.

The measured 0 and 90° peak shapes are shown in Figures 3a and 3b. Two components are evident in the peaks, a narrow central component and a broader less intense component at the wings of the peaks. The 0° peak is significantly broader than the 90° peak. More detailed information on the product angular distributions can be obtained by analyzing the 0 and 90° peaks to evaluate the asymmetry parameter. The methods used have been described in detail elsewhere.[12,14] The results of this analysis are summarized in Figure 3c where the asymmetry parameter, derived using a fifth-order polynomial, is plotted against the product relative kinetic energy. The dashed regions in Figure 3c indicate regions where the product intensity is less than 5% of the maximum and the values for the asymmetry parameter are unreliable. From Figure 3c it can be seen that the asymmetry parameter has values between 0.3 and 0.5 over the entire product kinetic energy range. The fit to the 0 and 90° peak shapes assuming a single value for the asymmetry parameter, $\beta = 0.4$, was only slightly less good than the fit shown in Figure 3a,b where we allowed β to vary with relative kinetic energy. This confirms that β does not vary substantially with product relative kinetic energy.

C. Photofragment Relative Kinetic Energies. Photofragment relative kinetic energy distributions are derived from Mn^+ peak shapes measured with the laser polarization at the "magic angle" of 54.7° with respect to the ion beam direction. With this orientation of the laser beam polarization the measured peak is independent of the product angular distribution and only contains information on the product relative kinetic energies.[13] Photofragment relative kinetic energy distributions derived from the magic angle peak shapes[13,16] are shown in Figure 4. The photofragment relative kinetic energy distribution for a wavelength

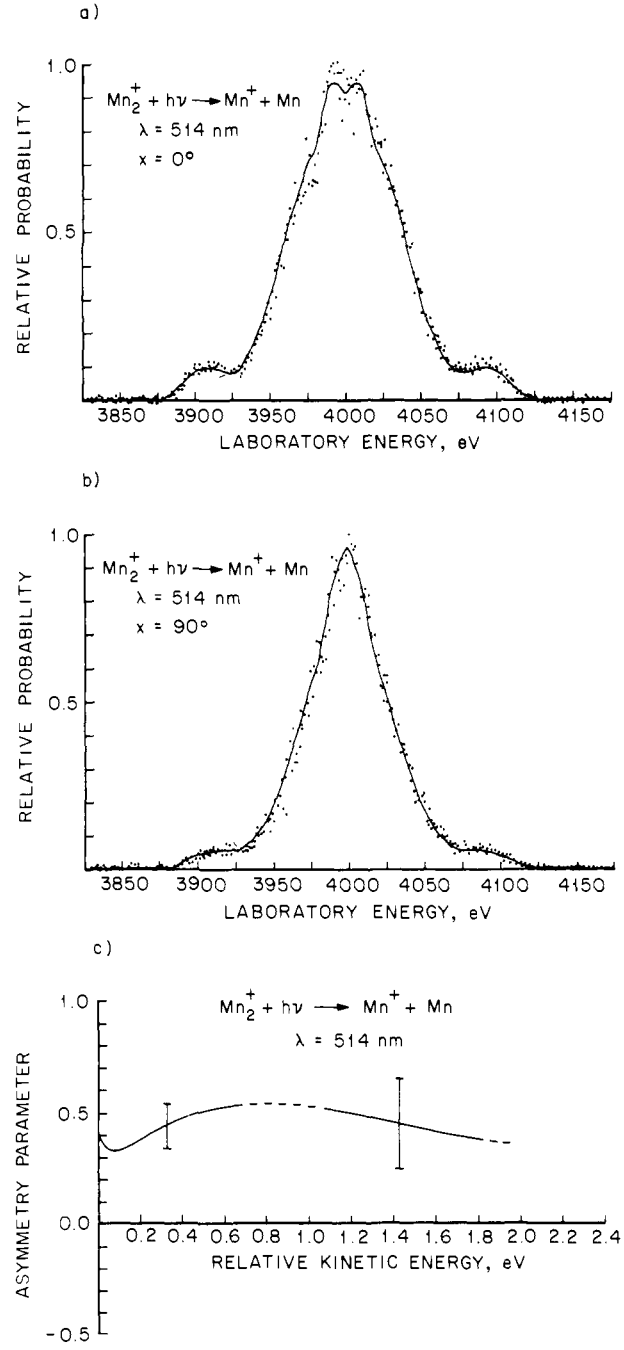

Figure 3. Peak shapes measured for the photodissociation of Mn_2^+ at 514 nm with the laser polarization at (a) 0° and (b) 90° with respect to the ion beam direction. The points are the experimental data, and the line is the result of the asymmetry parameter analysis (see text). (c) Plot of the asymmetry parameter against relative kinetic energy.

of 514 nm is shown in Figure 4a. The dashed line shows the distribution derived directly from the experimental data. The solid line shows the distribution corrected for instrumental discrimination. The discrimination arises mainly from the loss of ions with a large velocity component in the z direction owing to the finite slit heights. The procedure used to correct for discrimination was an improved version[18] of that given in ref 12. The remaining small excursions below zero in the distributions are due primarily to signal-to-noise problems, especially in Figure 4b where the signal was quite weak. These parts of the signals come from the shoulders on the peaks in Figure 3. A small part of the difficulty in Figure 4a,c could come from incomplete correction for dis-

(16) Jarrold, M. F.; Illies, A. J.; Kirchner, N. J.; Wagner-Redeker, W.; Bowers, M. T.; Mandich, M. L.; Beauchamp, J. L. *J. Phys. Chem.* **1983**, *87*, 2213, and references therein.

(17) Zare, R. N.; Herschbach, D. R. *Proc. IEEE* **1963**, *51*, 173. Zare, R. N. *Mol. Photochem.* **1972**, *4*, 1. Busch, G. E.; Wilson, K. R. *J. Chem. Phys.* **1972**, *56*, 3638. Yang, S.; Bersohn, R. *Ibid.* **1974**, *61*, 4400. Pernot, C.; Durup, J.; Ozenne, J.-B.; Beswick, J. A.; Cosby, P. C.; Moseley, J. T. *Ibid.* **1979**, *71*, 2387.

(18) Here an iterative procedure was employed so that the true distribution, rather than the measured distribution, was used to correct for discrimination.

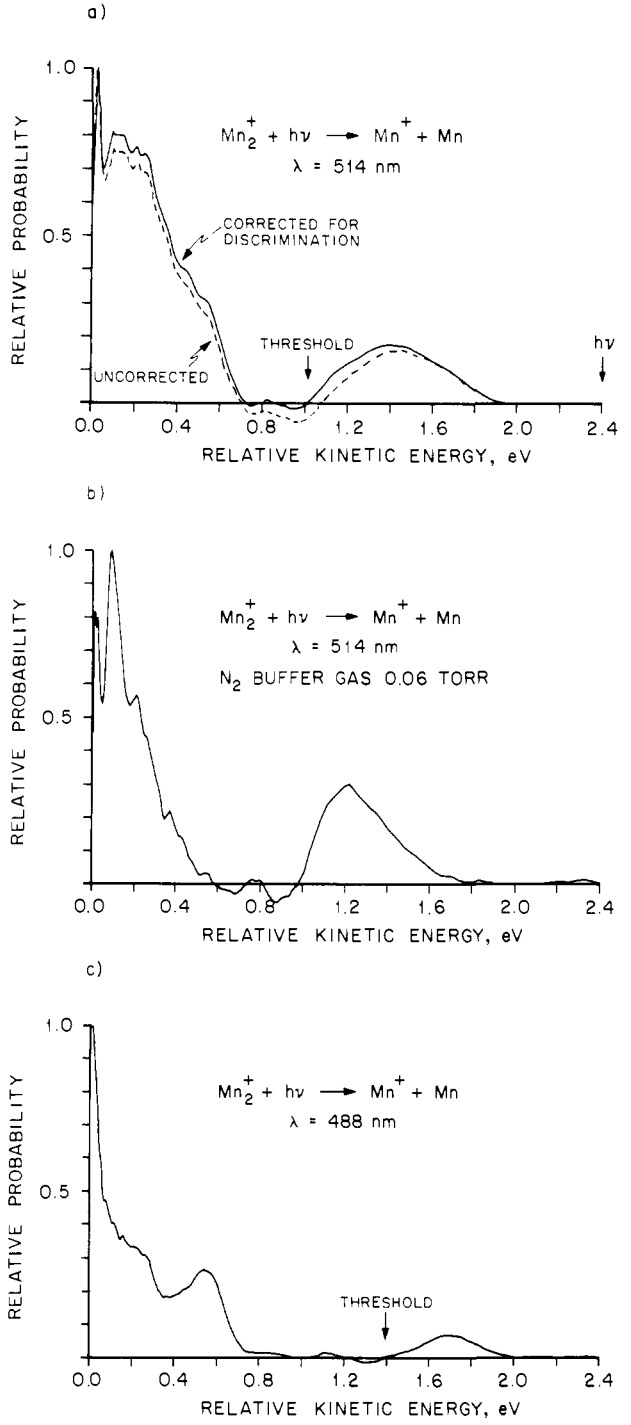

Figure 4. Product relative kinetic energy distributions for the photodissociation of Mn_2^+: (a) at 514 nm under EI conditions, (b) at 514 nm with 0.06 torr of N_2 buffer gas, and (c) at 488 nm under EI conditions.

crimination. The net effect would be a slight decrease in threshold and a slight increase in Mn_2^+ bond strength.

There are two components in the product relative kinetic energy distribution, a high-energy component with kinetic energies between 1.0 and 1.9 eV and a more intense lower energy component with kinetic energies between 0.0 and 0.7 eV. Figure 4b shows the product kinetic energy distribution measured at 514 nm with 0.06 torr of N_2 buffer gas in the source. It is apparent from the figures that the buffer gas increases the higher energy component relative to the lower energy component, and both the low- and high-energy components shift to lower relative kinetic energies.

Figure 4c shows the product relative kinetic energy distribution measured at 488 nm using EI conditions. Again, there are two components in the distribution. The high-energy component is less intense than at 514 nm, and the lower energy component has changed shape quite substantially. Distributions were also measured with other lines of the argon ion laser (502, 497, and 477 nm) and at 590 nm using the dye laser with R6G. All the distributions showed two components similar to the distributions shown in Figure 4.

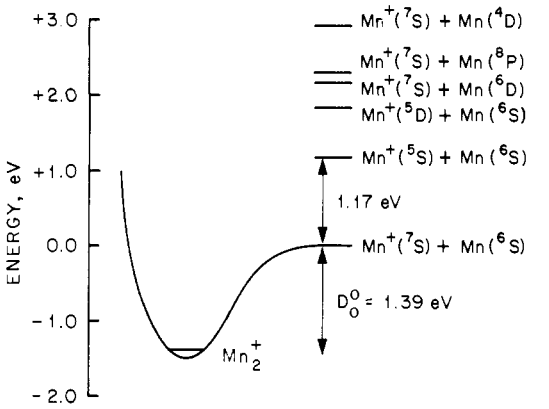

Figure 5. Potential energy diagram for Mn_2^+ constructed from data taken from ref 19 and the dissociation energy derived in the text.

IV. Discussion

A potential energy diagram for Mn_2^+ is shown in Figure 5. The data for Figure 5 were taken from ref 19, except for the dissociation energy of Mn_2^+ which is derived below from our measurements. As can be seen from Figure 5 there are a large number of excited electronic states with energies more than 1 eV above the ground-state products, $Mn^+(^7S) + Mn(^6S)$. The observed unimolecular "metastable" dissociation of Mn_2^+ must arise from a small fraction of the Mn_2^+ ions in the beam in a long-lived excited electronic state. Unfortunately, it is not possible to draw any firm conclusions about the origin of the "metastable" process because of the large density of Mn_2^+ excited electronic states and large number of possible product states. Judging from known first-row transition metal dimer vibrational frquencies,[20] the features in the metastable kinetic energy distribution separated by around 340 cm^{-1} could have a vibrational origin; i.e., the 340-cm^{-1} splitting corresponds to the separation between two vibrational levels in the excited state. However, the origin of the features separated by 800 cm^{-1} is more uncertain because this seems rather large (although perhaps not excessively so) for a first-row transition metal dimer vibrational frequency.

On photodissociation of Mn_2^+ there are only two ways in which the available energy can be disposed: product relative kinetic energy and electronic excitation of the products. As illustrated in the lower half of Figure 6 the separation between the two components in the photofragment relative kinetic energy distribution roughly corresponds to the energy separation between the ground state and first excited electronic state of the products. We therefore assign the product component with a large relative kinetic energy to the formation of ground-state products and the small kinetic energy component to the formation of excited electronic state products. It is likely that most of the excited-state products are in the first excited electronic state of the products: $Mn^+(^5S)$

(19) Moore, C. E. "Atomic Energy Levels", Vol. II, NSRDS-NBS 37; National Bureau of Standards: Washington, D. C., 1971.

(20) For example: (a) $V_2(X^3\Sigma_g^-)$ 535 cm^{-1}, $V_2(A^3\Pi_u)$ 640 cm^{-1} (Langridge-Smith, P. R. R.; Morse, M. D.; Hansen, G. P.; Smalley, R. E. *J. Chem. Phys.* **1984**, *80*, 593). (b) $Cr_2(X^1\Sigma_g^+)$ 452.3 cm^{-1} (Bondybey, V. E.; English, J. H. *Chem. Phys. Lett.* **1983**, *94*, 443). (c) $Cr_2(A^1\Sigma_u^+)$ 388.4 cm^{-1} (Michalopoulos, D. L.; Geusic, M. E.; Hansen, S. G.: Powers, D. E.; Smalley, R. E. *J. Phys. Chem.* **1982**, *86*, 3914). (d) $Mn_2(A^1\Sigma\mu^+)$ 111 cm^{-1}; $Fe_2(A)$ 194 cm^{-1}; $Fe_2(B)$ 218 cm^{-1}; $Ni_2(A)$ 192 cm^{-1} (DeVore, T.C.; Ewing, A.; Franzen, H. F.; Caldor, V. *Chem. Phys. Lett.*, **1975**, *35*, 78). (e) $Ni_2(X)$ 380.9 cm^{-1} (Ahmed, F.; Nixon, E. R. *J. Chem. Phys.* **1979**, *71*, 3547). (f) $Cu_2(X^1\Sigma_g^+)$ 266.1 cm^{-1} (Preuss, D. R.; Pace, S. A.; Gole, J. L. *Ibid.* **1979**, *71*, 3553). (g) $Cu_2(B^1\Sigma_u^+)$ 221 cm^{-1} (Gole, J. L.; English, J. H.; Bondybey, V. E. *J. Phys. Chem.* **1982**, *86*, 2560). (h) $Cu_2(A^3\Sigma_u^+)$ 125 cm^{-1} (Bondybey, V. E. *J. Chem. Phys.* **1982**, *77*, 3771). (i) $CuGa(X^1\Sigma)$ 220 cm^{-1}; $CuGa(A^1\Sigma)$ 117 cm^{-1} (Bondybey, V. E., Schwartz, G. P.; English, J. H., *Ibid.* **1983**, *78*, 11).

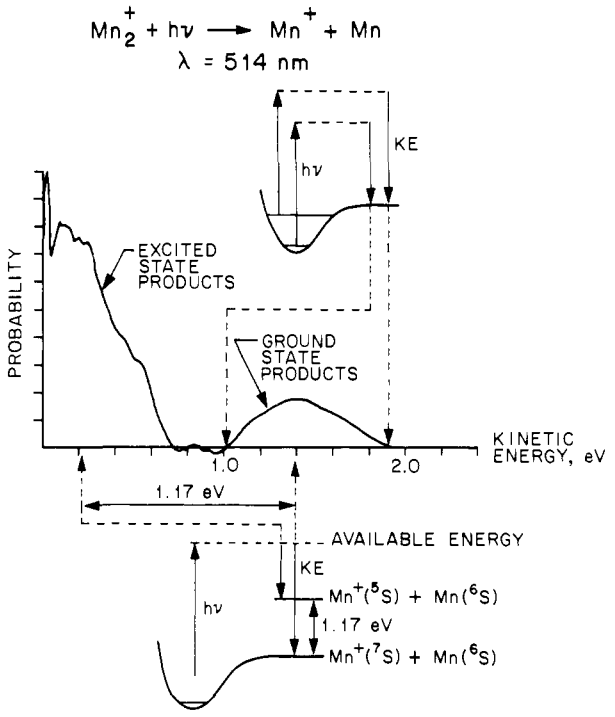

Figure 6. Diagram illustrating the formation of ground and excited electronic state products and the origin of the width of the high-energy component.

+ $Mn(^6S)$. However, we cannot rule out the possibility that some of these products are in more highly excited electronic states, and it is plausible that the sharp feature close to zero relative kinetic energy in the 488-nm photofragment distribution (see Figure 4c) arises from products in their second excited electronic state: $Mn^+(^5D)$ + $Mn(^+S)$.

As there are no internal modes, we would expect to see the photofragments have essentially single values of kinetic energy release corresponding to ground- and excited-state products. It is clear from Figure 4 that we see rather broad distributions. This occurs because the ground-state Mn_2^+ ions are internally excited. The product kinetic energies are then given by:

$$E_{KE} = h\nu - D^\circ_0(Mn^+\text{–}Mn) + E_{INT} - E_{ELEC} \qquad (2)$$

in which E_{INT} is the initial internal energy in Mn_2^+ and E_{ELEC} is the electronic excitation of the products. As is clear from eq 2 and illustrated in the upper half of Figure 6, products with large kinetic energies arise from internally excited reactant ions; that is, the product around 1.9 eV in Figure 6 arises from the photodissociation of vibrationally excited Mn_2^+ in its ground electronic state to give ground-state products, and products with ~1.0 eV kinetic energy arise from Mn_2^+ with less internal energy forming ground-state products. If the products at the kinetic energy threshold at 1.02 eV correspond to Mn_2^+ with no internal excitation, then this threshold will provide a measure of the dissociation energy of Mn_2^+ (see Figure 6). The dissociation energy is given by:

$$D^\circ_0(Mn^+\text{–}Mn) = h\nu - E_{thresh} \qquad (3)$$

where E_{thresh} is the kinetic energy threshold. The data given in Figure 4a yield a value of 1.39 eV for the dissociation energy of Mn_2^+.

When N_2 buffer gas is added to the ion source (see Figure 4b), the average intensity shifts to lower relative kinetic energy, and the higher energy component becomes larger relative to the lower energy component. These results suggest that the internal energy in the vibrationally excited Mn_2^+ ions is (partially) removed by collisions with the N_2 buffer gas. The threshold region in Figure 4b is relatively noisy because of the lower signal to noise with the buffer gas present (owing to the lower Mn_2^+ beam intensity). However, it is clear that the addition of the buffer gas does not significantly affect the location of the kinetic energy threshold. This result provides evidence that products at the kinetic energy threshold arise from the photodissociation of ground-state Mn_2^+.

Table I. Kinetic Energy Thresholds from the Distributions

wavelength, nm	E_{thresh}, eV	photon energy, eV	$D^\circ_0(Mn^+\text{–}Mn)$, eV lower limit[a]
590	0.85	2.10	1.25
514	1.02	2.41	1.39
502	1.32	2.47	1.15
497	1.44	2.49	1.05
488	1.39	2.54	1.15
477	1.46	2.60	1.14

[a] $h\nu - E_{thresh}$; see text.

At 488 nm the kinetic energy threshold is located at 1.39 eV (see Figure 4c). Using eq 3 this yields a value of 1.15 eV for $D^\circ_0(Mn^+\text{–}Mn)$. This value is significantly smaller than the value for $D^\circ_0(Mn^+\text{–}Mn)$ obtained at 514 nm. The data obtained at other wavelengths studied, along with the 514- and 488-nm data, are summarized in Table I. It is evident that the values for $D^\circ_0(Mn^+\text{–}Mn)$ vary quite substantially with wavelength. This point will be discussed further later in the paper.

We will first consider the photofragment angular distributions. These distributions provide information on the polarization of the electronic transition and on the lifetime of the excited ion relative to a rotational period.[17] The values of the asymmetry parameter for the photofragment angular distributions given in Figure 3c are around 0.4 for both ground and excited electronic state products. The asymmetry parameter can have values in the range $+2 > \beta > -1$, with +2 indicating a pure parallel transition and −1 indicating a pure perpendicular transition.[17] Values of the asymmetry parameter outside of the range $+0.5 > \beta > -0.25$ for a diatomic molecule indicate dissociation is rapid compared to a rotational period.[17] The interpretation of an asymmetry parameter with a value of +0.4 is ambiguous. There are two possible limiting interpretations: (1) a parallel transition with a lifetime greaer than a rotational period, and (2) a nearly equal mixture of parallel and perpendicular transitions with a lifetime much less than a rotational period. The first interpretation is probably more likely. However, regardless of the interpretation these results suggest that absorption of the photon does not initially access a short-lived repulsive state because a direct transition to a repulsive surface leading to ground-state products must be a parallel transition[21] and the value of β would have to be greater than 0.5. The photodissociation of Mn_2^+ thus probably involves transitions to one or more bound excited states followed by electronic predissociation to repulsive states leading to ground- and excited-state products.

Given the above result, the variation in the values of $D^\circ_0(Mn^+\text{–}Mn)$ with the wavelength evident in Table I can be understood in terms of the Franck-Condon factors for the transition to the intermediate bound excited state; as the wavelength changes the Franck-Condon factors change.[22] The largest value for $D^\circ_0(Mn^+\text{–}Mn)$ thus provides a rigorous lower limit to the true

(21) Since all molecular states correlating to ground-state product must be Σ states.

(22) A referee noted that if this were the case, a narrow peak might be expected rather than the 0.5-eV wide peak observed. With our experimental configuration the spectroscopic line widths will be due to the ions velocity distribution along the z direction (see Figure 1), which approximately corresponds to the thermal velocity distribution in the ion source. With 320K doppler limited spectroscopic line widths, we would expect to have several vibronic transitions at each laser wavelength because the Mn_2^+ ions have a large range of internal energies. The kinetic energy resolution in the center of mass frame varies with the product relative kinetic energy. At the threshold region it is around 0.05 eV so if there were several transitions we would not expect to resolve them in the kinetic energy distribution. Therefore, one narrow peak would not be expected, and we believe the 0.5-eV wide peak observed is an envelope of discrete vibronic transitions originating in the ground electron state smeared out by the relatively low kinetic energy resolution. While we believe the broad peak at high kineic energy release is due predominantly to ground electronic state ions, there is a large density of excited electronic states with asymptotic energies within several eV of the ground state. It is possible several of these are strongly bound and are within 0.5 eV of the ground state.

dissociation energy of Mn_2^+. The largest value in Table I is 1.39 eV obtained at 514 nm. This value is an average of four measurements with a statistical error of ±0.03 eV. The dissociation energy of Mn_2^+ is thus ≥1.39 eV (32 kcal mol^{-1}). From this result we derive a value for the adiabatic ionization potential for Mn_2 of $IP(Mn_2) \leq 6.47$ eV from the relationship

$$IP(Mn_2) = IP(Mn) + D°_0(Mn-Mn) - D°_0(Mn^+-Mn) \quad (4)$$

using IP(Mn) = 7.43 eV[19] and $D°_0(Mn_2) = 0.43$ eV.[7]

We assume in the above discussion that we are not photodissociating electronically excited Mn_2^+. From the observation of the "metastable" dissociation we know that a small fraction of the Mn_2^+ beam is in a long-lived excited electronic state. However, to be important in the photodissociation the electronically excited Mn_2^+ ions would have to make up a substantial proportion of the Mn_2^+ beam. There is no evidence from other studies that formation of Mn_2^+ from $Mn_2(CO)_{10}$ results in a substantial population in electronically excited states.[10,11] There appear to be no spin or symmetry restrictions to producing ground-state Mn_2^+ from $Mn_2(CO)_{10}$. Finally, the experiments with the buffer gas provide some evidence that we are sampling ground electronic state ions, although it is not clear how rapidly N_2 would quench electronically excited Mn_2^+.

The value for the metal-metal bond energy derived above $D°_0(Mn^+-Mn) \geq 1.39$ eV is substantially larger than that obtained by Ervin et al.[10] from the threshold for collision-induced dissociation of Mn_2^+. They derived a value of 0.85 ± 0.2 eV for the dissociation energy. In their experiment it is necessary to generate vibrationally cold ground-state ions, which they attempted to do using low-energy electron impact on $Mn_2(CO)_{10}$. It seems likely that a small fraction of their Mn_2^+ ions was vibrationally excited resulting in a low value for the dissociation energy of Mn_2^+ in their study.

V. Conclusions

The dimanganese ion from electron impact on $Mn_2(CO)_{10}$ photodissociates in the visible region of the spectrum. The photofragment relative kinetic energy distributions show that ground and excited electronic state products are produced and that some of the dimanganese ions are internally excited. Studies with N_2 buffer gas suggest that collisions with N_2 remove the internal energy from Mn_2^+. The photofragment angular distributions for both ground and excited electronic state products are characterized by an asymmetry parameter of $\beta = 0.4 \pm 0.1$ which suggests that photodissociation of Mn_2^+ occurs via an intermediate-bound excited state(s) which predissociates by a curve crossing mechanism. Analysis of the kinetic energy thresholds in the photofragment distributions leads to a rigorous lower limit for the metal-metal bond energy in Mn_2^+ of $D°_0(Mn^+-Mn) \geq 1.39$ eV and an adiabatic ionization potential for Mn_2 of $IP(Mn_2) \leq 6.47$ eV (assuming $D°_0(Mn_2) = 0.43$ eV).[7] The dissociation energy is larger than previously reported by Ervin et al. (0.85 ± 0.2 eV)[10] probably because their ions were internally excited.

Acknowledgment. We gratefully acknowledge the support of the Air Force Office of Scientific Research under Grant AFOSR82-0035 and the National Science Foundation under Grant CHE80-20464. We are also grateful for a number of useful discussions with Dr. Tony O'Keefe. Finally, We acknowledge useful conversations with Professor P. Armentrout on details of our source design.

The Electronic Spectrum of Cytosine

František Žaloudek, Joel S. Novros, and Leigh B. Clark*

Contribution from the Department of Chemistry, University of California, San Diego, La Jolla, California 92093. *Received October 9, 1984*

Abstract: Polarized reflection spectra in the range 360 to 135 nm taken from the (100) and (001) faces of single crystals of cytosine monohydrate have been interpreted through the Kramers-Kronig transformation in order to assign the polarization directions of six electronic transition moments of cytosine. Published linear dichroism studies of cytosine along with other crystal work are used to resolve the usual ambiguity in the interpretation of crystal spectra for the lowest three $\pi \rightarrow \pi^*$ transitions. An oriented gas analysis of the crystal spectra yield the following transition moment directions: $\theta_I = +6°$, $\theta_{II} = -46°$, $\theta_{III} = +76°$, $\theta_{IV} = -27°$ or 86°. Crystal field effects are considered in the dipole approximation in an effort to extract free molecule properties from the crystal data. Exciton mixing causes no large directional changes in moment directions; however, band components along the different crystal axes can show energy shifts of the order of 5000 cm^{-1}. Two higher energy features at 165 and 150 nm are discussed. The absorption spectrum polarized perpendicular to the molecular planes (obtained from reflection data taken from the (010) crystal face) shows no compelling evidence for an $n \rightarrow \pi^*$ transition at wavelengths longer than 225 nm.

There is at present considerable interest in the calculation of the optical properties of nucleic acids and polynucleotides.[1-3] Work is being directed in order to develop trustworthy ways of calculating the linear dichroism (LD) and circular dichroism (CD) for any particular polymer sequence and conformation. If the program is successful, then the comparison between such calculations and experimental CD and LD spectra will be useful in conformational deductions. Such studies, when taken together with structural information obtained with other methods, for example, NMR,[4] will surely reveal the physical nature and transformations of these polymers. Common to all approaches aimed at the optical properties is the need to understand the electronic states of the monomeric chromophores involved. Of special significance is a knowledge of the various monomer transition moment directions, for it is the mutual orientations of these moments which are of vital importance in the determination of the optical properties of the polymers. The experimentally known transition moment directions are either used directly in the calculations or employed to adjust and scale theoretically determined LCAO monopoles.

(1) See, for example the following review: Woody, R. W. *J. Polym. Sci.* **1977**, *12*, 181.
(2) Rizzo, V.; Schellman, J. A. *Biopolymers* **1984**, *23*, 435 and references therein.
(3) Matsuoka, Y.; Norden, B. *Biopolymers* **1983**, *22*, 1731.
(4) For a review of this important area see: Kearns, D. R. *Crit. Rev. Biochem.* **1984**, *15*, 237.

0002-7863/85/1507-7344$01.50/0